SPATIO-TEMPORAL FEW-SHOT LEARNING VIA DIFFUSIVE NEURAL NETWORK GENERATION

Yuan Yuan[*], **Chenyang Shao**[*], **Jingtao Ding**[†] **Depeng Jin, Yong Li**[†]
Department of Electronic Engineering,
BNRist, Tsinghua University,
Beijing, China
y-yuan20@mails.tsinghua.edu.cn, {dingjingtao, liyong07}@tsinghua.edu.cn

ABSTRACT

Spatio-temporal modeling is foundational for smart city applications, yet it is often hindered by data scarcity in many cities and regions. To bridge this gap, we propose a novel generative pre-training framework, GPD, for spatio-temporal few-shot learning with urban knowledge transfer. Unlike conventional approaches that heavily rely on common feature extraction or intricate few-shot learning designs, our solution takes a novel approach by performing generative pre-training on a collection of neural network parameters optimized with data from source cities. We recast spatio-temporal few-shot learning as pre-training a generative diffusion model, which generates tailored neural networks guided by prompts, allowing for adaptability to diverse data distributions and city-specific characteristics. GPD employs a Transformer-based denoising diffusion model, which is model-agnostic to integrate with powerful spatio-temporal neural networks. By addressing challenges arising from data gaps and the complexity of generalizing knowledge across cities, our framework consistently outperforms state-of-the-art baselines on multiple real-world datasets for tasks such as traffic speed prediction and crowd flow prediction. The implementation of our approach is available:
https://github.com/tsinghua-fib-lab/GPD.

1 INTRODUCTION

Spatio-temporal prediction is a fundamental problem in various smart city applications (Xia et al., 2024; Zhou et al., 2024; Wang et al., 2023a;c;b). Many deep learning models are proposed to solve this problem, whose successes however rely on large-scale spatio-temporal data. Due to imbalanced development levels and different data collection policies, urban spatio-temporal data, such as traffic and crowd flow data, are usually limited in many cities and regions. Under these circumstances, the model's transferability under data-scarce scenarios is of pressing importance.

To address this issue, various transfer learning approaches have emerged for spatio-temporal modeling. Their primary goal is to leverage knowledge and insights gained from one or multiple source cities and apply them effectively to a target city. These approaches can be broadly classified into two main categories. (1) Coarse-grained methods consider each city as a unified entity and transfer the learned knowledge at the city level (Pang et al., 2020; He et al., 2020; Ding et al., 2019; Tang et al., 2022). (2) Fine-grained methods dissect cities into smaller regions to enable a more refined exploration of region-level knowledge (Wang et al., 2019; Guo et al., 2018; Yao et al., 2019; Liu et al., 2021; Jin et al., 2022; Lu et al., 2022), which have shown better performance due to the inherent disparities between source and target cities. However, existing fine-grained methods largely rely on elaborated matching designs, such as utilizing auxiliary data for similarity calculation (Wang et al., 2019) or incorporating multi-task learning to obtain implicit representations (Lu et al., 2022). How to enable a more general knowledge transfer to automated retrieving similar characteristics across source and target cities still remains unsolved.

---

[*]Equal contribution.
[†]Corresponding author.

Recently, pre-trained models have yielded significant breakthroughs in the fields of Natural Language Processing (NLP) (Brown et al., 2020; Vaswani et al., 2017). Prompting techniques are also introduced to reduce the gap between fine-tuning and pre-training (Brown et al., 2020). At its core, the adoption of pre-trained models embodies the fundamental principles of transfer learning, allowing the model to acquire a broad understanding of various patterns and subsequently adapt to address specific tasks. Nowadays, what's particularly noteworthy is that advanced pre-trained models no longer require laborious fine-tuning, but leverage effective prompting techniques for fast adaptation (Brown et al., 2020; Rombach et al., 2022). Such capability serves as a crucial remedy for the current limitations in spatio—temporal few-shot learning, which offers the potential to enhance fine-grained transfer by general matching techniques.

However, despite these remarkable advancements of pre-trained models, there remains a notable gap in developing pre-trained models tailored for spatio-temporal scenarios. This disparity can be attributed to several challenges. Firstly, NLP benefits from a shared vocabulary that can be applied across various scenarios or tasks, while urban areas across different cities are geographically disjoint, lacking common elements that enable straightforward knowledge transfer. Secondly, substantial divergence often exists in data distributions between source and target cities, leading to the potential noise or even counterproductive information in the knowledge acquired from source cities (Jin et al., 2022). Additionally, pattern divergence exists even within one city due to regions with different functions. These divergences pose challenges to the effective transfer of knowledge to a target city. In other words, the knowledge obtained from the data often contains noise and bias, making it hard to train a universal model that perfectly fits patterns with high variations in different cities. Achieving effective transfer in this context requires addressing a more complex setting of generalization across cities. The key challenge, therefore, lies in determining what transferable knowledge, analogous to the shared semantic structure in NLP, can be established for urban settings.

In this work, we present a generative pre-training framework for spatio-temporal few-shot learning. Instead of fitting the spatio-temporal data with a unified model, we propose a novel pre-training strategy that captures universal patterns from optimized neural network parameters. In simpler terms, we recast spatio-temporal few-shot learning as pre-training a generative hypernetwork. This hypernetwork is designed to adaptively generate unique parameters for spatio-temporal prediction models guided by prompts.

Essentially, our pre-training approach empowers the capability to adaptively generate distinctive neural networks in response to diverse data distributions, which addresses the challenges arising from data gaps across cities or regions. To elaborate, we begin with a set of neural networks optimized for spatio-temporal predictions. Then we design a Transformer-based diffusion model to generate network parameters from Gaussian noise conditioned on the prompt. We also design a class of conditioning strategies for the prompt to guide the denoising process. Consequently, when presented with a target prompt encoding spatio-temporal characteristics of the target scenario, the diffusion model generates corresponding neural networks for accurate predictions. Our framework is model-agnostic, ensuring compatibility with state-of-the-art spatio-temporal prediction models. We summarize our contributions as follows:

- We propose to leverage pre-training paradigm to achieve effective fine-grained spatio-temporal knowledge transfer across different cities, which stands as a pioneering practice in handling urban data-scarce scenarios with pretrained models.

- We propose a novel **G**enerative **P**re-training framework based on **D**iffusion models, called GPD. It leverages a Transformer-based diffusion model and city-specific prompts to generate neural networks, opening new possibilities for improving spatio-temporal modeling.

- Extensive experiments on multiple real-world scenarios demonstrate that GPD achieves superior performance towards data-scarce scenarios with an average improvement of 7.87% over the best baseline on four datasets.

2 RELATED WORKS

Spatio-Temporal Few-Shot Learning. Addressing data scarcity is a pervasive challenge in machine learning-driven urban computing applications (Wei et al., 2016; He et al., 2020; Zhou et al., 2023a). This issue is particularly pronounced in cities lacking advanced digital infrastructure or in

the initial stages of deploying sensors, as they struggle to accumulate adequate data. To solve these issues, spatio-temporal few-shot learning (Zhuang et al., 2020) has emerged as a promising solution. Existing solutions can be broadly categorized into coarse-grained and fine-grained methods. Coarse-grained methods (Fang et al., 2022; Liu et al., 2018; Pang et al., 2020; He et al., 2020; Ding et al., 2019; Tang et al., 2022; Yao et al., 2019) treat each city as a whole and apply transfer learning techniques, such as adversarial learning (Fang et al., 2022) and meta-learning (Yao et al., 2019), to leverage knowledge across urban contexts. Differently, fine-grained methods (Wang et al., 2019; Guo et al., 2018; Liu et al., 2021; Jin et al., 2022) divide cities into smaller regions and identify similar region pairs for knowledge transfer. They use various techniques, such as Similarity-based matching (Wang et al., 2019) or re-weighting (Jin et al., 2022), to facilitate the transfer of insights between these regions. Fine-grained methods have demonstrated better performance due to the inherent disparities between source and target cities (Jin et al., 2022). (Lu et al., 2022) proposed to learn meta-knowledge to facilitate node-level knowledge transfer. Instead, we propose a generative pre-training framework made up of a diffusion-based hypernetwork and adaptive conditioning strategy. Our framework not only exhibits powerful parameter generation capabilities but also offers remarkable flexibility by allowing the use of various forms of prompts.

Diffusion Models. Diffusion probabilistic models (Ho et al., 2020; Song et al., 2020; Nichol & Dhariwal, 2021) have emerged as a powerful alternative to generation tasks, which not only outperform Generative Adversarial Networks (Goodfellow et al., 2020) on image generation tasks with higher fidelity (Dhariwal & Nichol, 2021; Rombach et al., 2022), but also enable effective crossmodal conditioning (Bao et al., 2023; Nichol et al., 2022). In addition to image generation, diffusion models have also been utilized for other tasks, such as video generation (Ho et al., 2022; Luo et al., 2023), text generation (Li et al., 2022; Gong et al., 2022), implicit neural fields generation (Erkoç et al., 2023), network learning (Peebles et al., 2022), graph generation (Vignac et al., 2023), and spatio-temporal prediction (Wen et al., 2023; Yuan et al., 2023). In contrast, our approach leverages diffusion models to generate neural network parameters of spatio-temporal prediction models.

Hypernetworks. Hypernetworks represent a class of generative models tasked with producing parameters for other neural networks (Ha et al., 2017). These hypernetworks serve two primary purposes: (1) the generation of task-specific parameters (Ha et al., 2017; Alaluf et al., 2022), where hypernetworks are usually jointly trained with specific task objectives, and (2) the exploration of neural network characteristics (Schürholt et al., 2022; 2021), which focus on learning representations of neural network weights to gain insights of network properties. In our work, we align with the first purpose, focusing on the generation of parameters tailored to the target city for spatio-temporal prediction. There are also hypernetworks for spatio-temporal prediction (Pan et al., 2019; Bai et al., 2020; Pan et al., 2020; 2018; Li et al., 2023), which use non-shared parameters for different nodes. Our key differences lie in three aspects. Firstly, our framework ensures compatibility with state-of-the-art models, while those works propose specific model designs. Secondly, different from the pre-training solution (Li et al., 2023) with a mask autoencoder, we focus on the pre-training of model parameters. Thirdly, our approach is a spatio-temporal few-shot learning framework, capable of acquiring knowledge from multiple cities and effectively transferring it to few-shot scenarios. In contrast, those works have certain limitations in data-scarce urban environments.

3 PROPOSED METHOD

3.1 PRELIMINARY

We introduce some preliminaries related to our research problem.

Definition 1 (Spatio-Temporal Graph). *A spatio-temporal graph (STG) as $\mathcal{G}_{ST} = (\mathcal{V}, \mathcal{E}, \mathcal{A}, \mathcal{X})$, where $\mathcal{V}$ is the node set, $\mathcal{E}$ is the edge set, $\mathcal{A}$ is the adjacency matrix, and $\mathcal{X}$ denotes the node feature. The node features can encompass various aspects such as crowd flows and traffic speed.*

For example, for the crowd flow dataset, nodes correspond to segmented regions within the city, with edges indicating their geographic adjacency. For the traffic speed dataset, nodes represent the sensors deployed along the road network, and edges signify the connections between these sensors. The construction of the spatio-temporal graph is adaptable to the specific requirements of each task.

Problem 1 (Spatio-Temporal Prediction). *For a spatio-temporal graph $\mathcal{G}_{ST}$, suppose we have L historical signals $[X^{t-L+1}, X^{t-L+2}, \ldots, X^t]$ for each node and predict the future n steps*
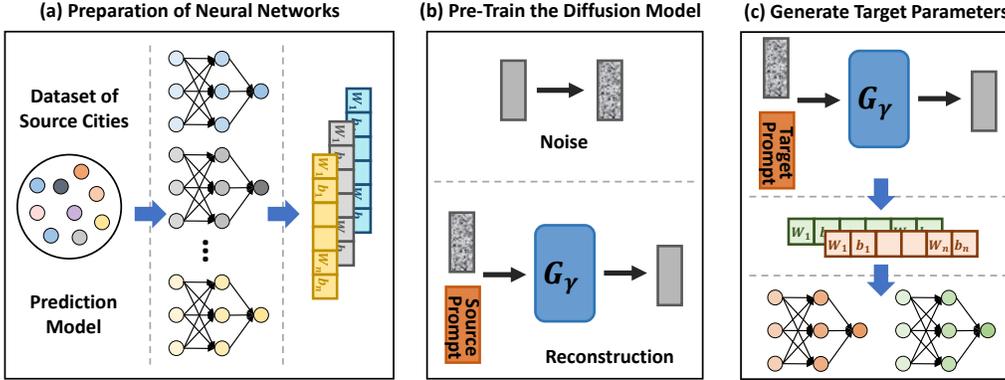
Figure 1: An overview of the proposed framework. (a) A collection of optimized spatio-temporal prediction models based on the dataset of source cities; each model's parameters are transformed into a vector-based format. (b) Pre-training the diffusion model to generate neural network parameters from the noise given the prompt. (c) Utilizing the pre-trained diffusion model to generate neural network parameters for the target city based on the target prompt.

$[X^{t+1}, \ldots, X^{t+n}]$. *The prediction task is formulated as learning a θ-parameterized model F given a spatio-temporal graph $\mathcal{G}_{ST}$:* $[X^{t+1}, \ldots, X^{t+n}] = F_\theta(X^{t-L+1}, X^{t-L+2}, \ldots, X^t; \mathcal{G}_{ST})$.

Problem 2 (Spatio-Temporal Few-Shot Learning). *Spatio-temporal few-shot learning is formulated as learning knowledge $\mathcal{K}$ from source cities $\mathcal{C}_{1:P}^{source} = \{\mathcal{C}_1^{source}, \ldots, \mathcal{C}_P^{source}\}$, and then transfer the learned knowledge $\mathcal{K}$ to the target city with few-shot structured data to facilitate spatio-temporal predictions.*

Problem 3. *We formulate the spatio-temporal few-shot learning as pre-training a diffusion model to conditionally generates neural network parameters, and then utilizing it to generate parameters for the target city's prediction model. Suppose we have a collective of learned prediction models $F = \{F_{\theta_1}, F_{\theta_2}, \ldots, F_{\theta_N}\}$ from a set of data-rich source cities $\mathcal{C}_{1:P}^{source} = \{\mathcal{C}_1^{source}, \ldots, \mathcal{C}_P^{source}\}$, we aim to pre-train a diffusion model to generate F with source-city prompts. The optimized diffusion model serves as the learned knowledge $\mathcal{K}$, which can be transferred to the target city.*

3.2 OVERALL FRAMEWORK

Figure 1 provides an illustrative overview of our proposed framework, which contains three phases. The left part shows the preparation of model parameters, from which we can obtain a collection of optimized neural network parameters. The middle part illustrates the pre-training phase within source cities, where the diffusion model G_γ is trained to generate meaningful parameters from Gaussian noise given source prompts. The right part demonstrates the how we transfer the learned diffusion model to facilitate spatio-temporal predictions in the target city. In the following subsections, we elaborate on the details of these phases.

3.3 SPATIO-TEMPORAL PREDICTION MODEL

Our framework is model-agnostic, ensuring compatibility with state-of-the-art spatio-temporal prediction models. Here we utilize well-established STG models, specifically STGCN (Yu et al., 2017) and GWN (Wu et al., 2019), and MLP-based model STID (Shao et al., 2022a) , as prediction models[1]. In this work, we train the prediction model (denoted as F_{θ_i}) separately for each region within a given city.

3.4 GENERATIVE PRE-TRAINING ON PARAMETER SPACE

Our approach is a conditional generative framework designed to directly learn from model parameters of source cities. This pre-training process enables the generation of new model parameters for target cities. Our training paradigm encompasses a three-phase approach as follows.

---

[1]Appendix A.4 provides more details of the three models.

Preparation of Neural Networks. As the initial step, we optimize spatio-temporal prediction models for each region within source cities and save their optimized network parameters. It's important to note that, while we use the same network architecture for different regions, each set of model parameters is uniquely optimized for its respective region. In other words, there is no parameter sharing, and each model is meticulously trained to achieve peak performance specific to its region. This optimization process can be formulated as follows:

$$\theta_i = \arg\min_{\theta_i} \sum_t \left\| f_{\theta_i}(X_i^{t-L+1}, X_i^{t-L+2}, \ldots, X_i^t; \mathcal{G}_{ST}) - [X^{t+1}, \ldots, X^{t+n}] \right\|^2,$$

$$\mathcal{T}(\theta) = \{\theta_1, \theta_2, \ldots, \theta_M\}, M = \sum_{s=1,\ldots,N} n_s,$$

where i denotes the i_{th} region within a source city, and θ_i represents parameters of its dedicated prediction model. N denotes the total number of source cities, and n_s indicates the number of regions in source city s. $\mathcal{T}(\theta)$ encompasses the optimized parameters of prediction models.

To optimize these parameters, we employ the standard Adam optimizer. These meticulously optimized parameters serve as the ground truth for the subsequent generative pre-training process. Algorithm 1 in Appendix A.5 illustrates the training process. Then we transform the parameters of each model into a vector-based format.

Generative Pre-Training of the Diffusion Model. Using the dataset comprising pre-trained parameters of prediction models and region prompts, we employ a generative model denoted as G_γ to learn the process of generating model parameters in a single pass. Specifically, G_γ predicts the distribution of parameters $p_G(\theta_i|p_i)$, where p_i corresponds to the prompt of region i. We adopt diffusion models (Ho et al., 2020) as our generative model due to its efficacy in various generation tasks (Ho et al., 2022; Li et al., 2022; Vignac et al., 2023). Moreover, it has shown superior performance on multi-modal conditional generation (Bao et al., 2023; Nichol et al., 2022; Saharia et al., 2022).

We train the diffusion model to sample parameters by gradually denoising the vector from the Gaussian noise. This process is intuitively reasonable as it intriguingly mirrors the optimization journey from random initialization which is a well-established practice in existing optimizers like Adam. Our model takes two parts as the input: a noise-corrupted parameter vector θ^k and a region prompt p, with k representing the step in the forward diffusion process. The training objective is as follows:

$$\mathcal{L} = \mathbb{E}_{\theta^0, \epsilon \sim \mathcal{N}(0,1), k}[\|\epsilon - \epsilon_\gamma(\boldsymbol{\theta}^k, p, k)\|^2], \tag{1}$$

where ϵ denotes the noise to obtain θ^k from θ^0. Algorithm 2 illustrates the pre-training procedure.

Sampling. After pre-training, we can generate parameters θ_i by querying G_γ using a region prompt p for the target cities. When the region prompt in the target city closely resembles a region in multiple source cities, we can seamlessly approximate the model parameters specific to the target domain. In essence, we harness the power of the prompt to facilitate efficient knowledge transfer and precise parameter matching, which leverages the inherent similarities between regions across cities. The generation is an iterative sampling process from step $k = K$ to $k = 0$, which denoises the Gaussian noise into meaningful parameters. The generation process is formulated as follows:

$$\boldsymbol{\theta}^{k-1} = \frac{1}{\sqrt{\alpha_k}}(\boldsymbol{\theta}^k - \frac{\beta_k}{\sqrt{1 - \overline{\alpha}_k}}\epsilon_\gamma(\boldsymbol{\theta}^k, p, k)) + \sqrt{\sigma_\gamma}\mathbf{z}, \tag{2}$$

where $\mathbf{z} \sim \mathcal{N}(\mathbf{0}, \boldsymbol{I})$ for $k > 1$ and $\mathbf{z} = \mathbf{0}$ for $k = 1$. Algorithm 3 illustrates the procedure.

3.5 ARCHITECTURE

The generative model is a transformer-based diffusion architecture that learns the relationships across different layers of the prediction model via effective self-attention. It has been shown that the Transformer can effectively capture relationships of each token in long sequences. We find it to be a good choice to learn inter-layer and intra-layer interactions.
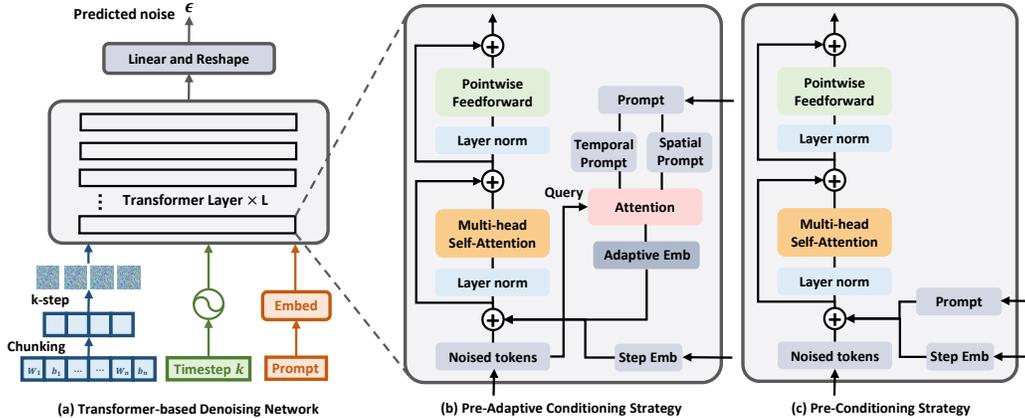
Figure 2: The network architecture of the denoising network. (b) and (c) illustrate two conditioning strategies, and we provide other used conditioning strategists in Appendix A.3.

Parameter Tokenizers. Spatio-temporal prediction models always exhibit complicated architectures consisting of various neural network layers, such as temporal layers, spatial layers, and spatio-temporal interaction layers. Usually, these layers are characterized by different shapes. These heterogeneous layer structures pose a challenge if we want to leverage the Transformer model to capture intricate relationships between them. To provide a clearer conceptual understanding, Table 4 and Table 5 in Appendix A.4 illustrate the layer structures of an spatio-temporal model. It is evident that different layers possess parameter tensors of diverse shapes. Therefore, it is necessary to decompose these parameters into vector-based tokens of uniform dimensions while preserving the inherent connectivity relationships within the original prediction model.

We achieve this by determining the greatest common divisor (denoted as g) of the parameters amount across all layers, then we perform layer segmentation by reshaping each layer into several tokens as: $n_m = N_m/g$, where n_m is the number of tokens for the layer m and N_m is the number of parameters of the layer m. After that, the tokens are connected in a sequential manner, ensuring that layers that are adjacent in the network structure also maintain adjacency within the resulting sequence. This systematic approach facilitates the effective utilization of Transformer-based architectures in handling spatio-temporal prediction models with heterogeneous layer structures.

Region Prompt. The selection of region prompts offers flexibility, as long as they can capture the distinctive characteristics of a specific region. Various static features, such as population, region area, function, and distribution of points of interest (POI), can be leveraged for this purpose. In this work, we utilize region prompts from two aspects: spatial and temporal domains. For the spatial prompt, we utilize node embeddings extracted from a pre-trained knowledge graph. It only utilizes relations like region adjacency and functional similarity, which are easily obtained in all cities. Simultaneously, we employ self-supervised learning techniques (Shao et al., 2022b) on the very limited time series data (three days) to derive the embedding for the temporal prompt. Appendix A.2 provides more details of the prompt design.

Denoising Network. Figure 2 demonstrates the architecture of the denoising network, which adopts a prompt-based transformer diffusion model. After the layer segmentation, the parameters are restructured into a token sequence. In the denoising process, the transformer layers operate on the noised token sequence. In addition to the noised sequence, our transformer diffusion model also takes in the timestep k and region prompt p. We anticipate that the model is capable of generating outputs conditioned on the region prompt. To this end, we explore several conditioning approaches, which introduce small but important modifications to the standard transformer layer design. The conditioning strategies are shown in Figure 2(b) and 2(c). We also explore more conditioning strategies, such as "Post-adaptive conditioning" and "Adaptive norm conditioning" (see Appendix A.3).

- **Pre-conditioning.** "Pre" denotes that the prompt is integrated into the token sequence before being fed into self-attention layers. In this conditioning strategy, we simply add the spatial prompt and temporal prompt into a spatio-temporal prompt. Then, we uniformly add it to each token. This design allows us to leverage standard transformer layers without requiring any modifications.

- **Pre-conditioning with inductive bias.** When adding the vector embeddings of k and p to the token embeddings, we introduce inductive bias: the timestep vector is added uniformly to each token, while the spatial prompt and temporal prompt are incorporated into spatial-related and temporal-related parameters, respectively. Inductive bias can be introduced flexibly based on the used spatio-temporal model architectures.

- **Pre-adaptive conditioning.** In this variant, the operation on the timestep embedding remains the same. However, concerning the prompt, we treat the embeddings of p as a two-element sequence. An attention layer is introduced to realize the "adaptive" mechanism, dynamically determining to what extent the prompt should be added to specific token embeddings. This approach aims to empower the model to learn how to adaptively utilize the prompts, enhancing its conditioning capabilities.

4 EXPERIMENTS

4.1 EXPERIMENTAL SETUP

Datasets. We conduct experiments on two types of spatio-temporal prediction tasks: crowd flow prediction and traffic speed prediction. As for crowd flow prediction, we conducted experiments on three real-world datasets, including New York City, Washington, D.C., and Baltimore. Each dataset contains hourly urban flow of all regions, and we use half of the day (12 hours) as a training sample. As for traffic speed prediction, we conduct experiments on four real-world datasets, including Meta-LA, PEMS-BAy, Didi-Chengdu, and Didi-Shenzhen. Their time intervals are 5min, 5min, 10min, and 10min. We use 12 points as a training sample. For both tasks, we categorized the datasets into source cities and one target city. For example, if one specific city is set as the target dataset, we assume access to only a limited quantity of data, such as three-day data (existing models usually require several months of data to train the model). The diffusion model is trained using the other source cities with rich data. This same division and training strategy is consistently applied when targeting different cities. Appendix B.1 provides more details of the used datasets.

Baselines and Metrics. To evaluate the performance of our proposed framework, we compare it against classic models and state-of-the-art urban transfer approaches, including History Average (HA), ARIMA, RegionTrans (Wang et al., 2019), DASTNet (Tang et al., 2022), AdaRNN (Du et al., 2021), MAML (Finn et al., 2017), TPB (Liu et al., 2023), and ST-GFSL (Lu et al., 2022). We use two widely-used regression metrics: Mean Absolute Error (MAE) and Root Mean Squared Error (RMSE). Appendix B.2 and B.3 provide more details of baselines and implementation.

4.2 RESULTS

Performance Comparison. We compare the performance of our proposed GPD with baselines on two tasks: crowd flow prediction and traffic speed prediction. In both tasks, our goal is to transfer knowledge from the source cities to the target city. Due to space limits, Table 1 only reports the comparison results for the mean error of prediction over the subsequent 6 steps for some datasets. Comprehensive evaluations, including step-wise performance on all datasets, can be found in Appendix C. Based on these results, we have these noteworthy observations:

- **Consistent Superiority.** GPD consistently achieves the best performance compared with baseline approaches. When compared against the best-performing baselines (indicated by underlining in Table 1), GPD achieves an average error reduction of 4.31%, 17.1%, 2.1% and 8.17% in terms of MAE for Washington D.C., Baltimore, LA, and Chengdu. These improvements indicate that GPD enables effective knowledge transfer regarding parameter generation.

- **Competitive Long-Term Prediction.** GPD exhibits its competitiveness particularly in long-term prediction scenarios, as shown in Tables in Appendix C. For example, when considering Baltimore as the target city (Appendix Table 11), compared with the state-of-the-art baseline STGFSL, GPD shows an improvement in MAE performance of up to 22.1% at the 6_{th} step, compared to a 5.9% improvement at the 1_{st} step. This notable trend can be attributed to the inherent design of our framework, which facilitates the transfer of long-term temporal knowledge to the target city.

Performance across Cities. To investigate the influence of different source cities on our experimental outcomes, we conducted a series of experiments using various source cities for the target

Model	Washington D.C.		Baltimore		LA		Didi-Chengdu	
	MAE	RMSE	MAE	RMSE	MAE	RMSE	MAE	RMSE
HA	21.520	47.122	15.082	26.768	3.257	6.547	3.142	4.535
ARIMA	19.164	42.480	12.902	23.758	7.184	10.91	5.381	7.087
RegionTrans	13.853	31.951	7.375	<u>13.715</u>	3.349	5.728	2.828	4.130
DASTNet	14.808	32.219	7.532	13.975	3.236	5.603	2.810	3.953
MAML	13.930	31.009	7.978	14.901	3.257	5.558	2.874	4.041
TPB	13.552	31.024	7.421	14.011	3.198	<u>5.574</u>	2.654	<u>3.709</u>
STGFSL	<u>12.224</u>	<u>28.625</u>	<u>7.365</u>	13.746	<u>3.184</u>	5.577	<u>2.570</u>	3.832
GPD (ours)	**11.697**	**27.308**	**6.110**	**11.669**	**3.119**	**5.450**	**2.366**	**3.393**
Reduction%	**-4.31%**	**-4.62%**	**-17.1%**	**-14.9%**	**-2.1%**	**-3.2%**	**-8.17%**	**-8.62%**

Table 1: Performance comparison of few-shot scenarios on two crowd flow datasets (Washington D.C. and Baltimore) and two traffic speed datasets (LA and Didi-Chengdu) in terms of MAE and RMSE. We use the average prediction errors over six steps as the result. Bold denotes the best results and <u>underline</u> denotes the second-best results.

Target city	Source city	MAE					
		Step 1	Step 2	Step 3	Step 4	Step 5	Step 6
Washington D.C.	B	29.039	28.226	29.358	28.146	30.026	31.268
	N	27.569	28.631	27.285	28.229	27.858	29.667
	B+N	26.679	26.624	26.27	26.262	26.639	26.112
Baltimore	W	15.492	15.676	15.575	17.213	17.915	17.338
	N	17.234	17.737	17.395	17.325	18.734	18.179
	W+N	15.259	14.219	14.309	15.334	14.68	14.876
NYC	W	51.344	54.478	50.078	49.87	48.612	52.143
	B	53.145	51.088	48.292	54.658	62.494	60.525
	W+B	42.337	42.392	42.417	42.304	42.312	42.28

Table 2: Performace comparison with different source cities for crowd flow predictions. "W", "B", and "N" represent Washington D.C., Baltimore, and NYC, respectively.

city. For instance, when considering Washington D.C. as the target city, we analyzed three distinct source city scenarios: (1) using New York City (N) as the source city, (2) utilizing Baltimore (B) as the source city, and (3) incorporating both NYC and Baltimore (N+B) as source cities. The results summarized in Table 2 indicate that incorporating data from multiple source cities offers substantial benefits for both short-term and long-term predictions across all three target cities. This suggests that our framework effectively learned useful and transferable knowledge from these source cities. In one-step predictions, the inclusion of two source cities, as opposed to just one, results in performance improvements: 8.1% and 3.2% for Washington, 1.5% and 11.4% for Baltimore, and 17.5% and 20.3% for NYC. When extending our analysis to six-step predictions, the advantages of utilizing two source cities over one are even more pronounced, with performance improvements of 16.4% and 12.0% for Washington, 14.2% and 18.1% for Baltimore, and 18.9% and 30.1% for NYC. These results emphasize the significance of leveraging data from multiple source cities for the pre-training.

4.3 FLEXIBILITY OF GPD

Our framework is designed to be model-agnostic, providing support for cutting-edge spatio-temporal models. To validate the versatility of our framework, we also integrated another two advanced spatio-temporal prediction models, Graph WaveNet (GWN) (Wu et al., 2019) and Spatial-Temporal Identity (STID) (Shao et al., 2022a), into our framework. Specifically, STGCN and GWN are graph-based architectures, while STID does not leverage graph neural networks.

Figure 7 in Appendix presents a comprehensive performance comparison across the three spatio-temporal models—STGCN, GWN, and STID—across four datasets encompassing both crowd flow prediction and traffic speed prediction. The results reveal that STGCN and GWN exhibit nearly comparable performance, with GWN slightly outperforming. STID, given its relatively simpler design
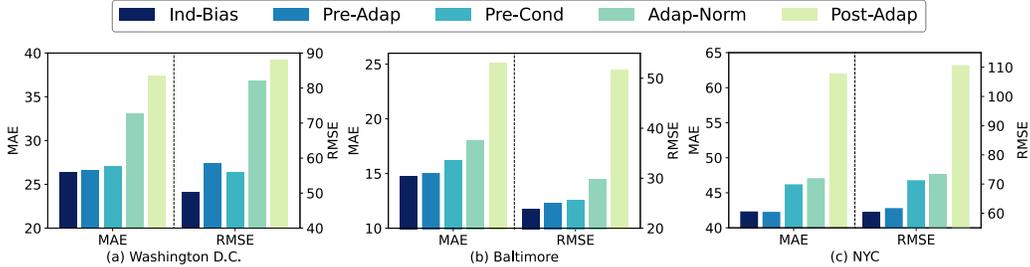
Figure 3: Performance comparison across different conditioning strategies.

and potential limitations in modeling complex spatio-temporal relationships, lags slightly behind STGCN and GWN. Therefore, we implement GWN as the base model for baselines to examine the effectiveness of our framework. Appendix C.1 provides the detailed comparison results. This comparison underscores our framework's adaptability to integrate existing spatio-temporal models and its inherent potential to enhance prediction performance, particularly as more powerful models become available.

4.4 IN-DEPTH STUDY OF GPD

Conditioning Strategy. We investigate how the conditioning strategies affect the model's performance. Figure 3 presents the comparison results. As we can observe, inducing inductive bias to the conditioning strategy consistently leads to lower prediction errors compared to other conditioning approaches across various datasets. The second-best performing strategy is the "Adaptive Sum of Prompts", which employs an attention mechanism to flexibly aggregate prompts related to different aspects for each token. This approach exhibits promise in addressing diverse spatio-temporal models in a general and flexible manner. Conversely, the conditioning strategy without self-attention operation demonstrates the poorest performance. This outcome indicates the importance of incorporating the prompt within the Transformer's self-attention layers for the generative pre-training process.

Prompts. We conduct experiments to investigate the influence of prompt selection on the final performance. Figure 4 illustrates the comparison results of three prompt methods: the spatio-temporal prompt (ours), the spatial prompt (w/o temporal), and the temporal prompt (w/o spatial). As we can observe, eliminating either the spatial or temporal prompt leads to a reduction in the model's performance, while employing both the spatio-temporal prompt yields the most favorable performance. These findings underscore the significance of harnessing the characteristics of the target city from both spatial and temporal perspectives in the context of spatio-temporal prediction.
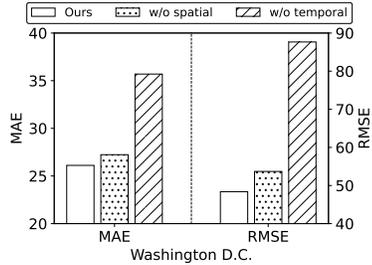
Figure 4: Performance comparison of different prompts with Washington D.C. as the target city.

5 CONCLUSION

GPD introduces a pioneering generative pre-training framework for spatio-temporal few-shot learning, addressing the challenges posed by data scarcity and heterogeneity in smart city applications. By conducting pre-training in the parameter space, GPD addresses the inherent disparities present in the data space across different cities and enables a new but effective knowledge transfer. Its model-agnostic nature ensures compatibility with existing urban computing models, making it a valuable tool for researchers and practitioners in the field. Our framework represents a significant advancement in urban transfer learning, which has the potential to revolutionize smart city applications in data-scarce environments and contribute to more sustainable and efficient urban development. As for future work, researchers can explore more sophisticated methods for prompt selection, such as leveraging large language models to capture the unique characteristics of cities.

REFERENCES

Yuval Alaluf, Omer Tov, Ron Mokady, Rinon Gal, and Amit Bermano. Hyperstyle: Stylegan inversion with hypernetworks for real image editing. In *Proceedings of the IEEE/CVF conference on computer Vision and pattern recognition*, pp. 18511–18521, 2022.

Lei Bai, Lina Yao, Can Li, Xianzhi Wang, and Can Wang. Adaptive graph convolutional recurrent network for traffic forecasting. *Advances in neural information processing systems*, 33:17804–17815, 2020.

Ivana Balažević, Carl Allen, and Timothy M Hospedales. Tucker: Tensor factorization for knowledge graph completion. *arXiv preprint arXiv:1901.09590*, 2019.

Fan Bao, Shen Nie, Kaiwen Xue, Chongxuan Li, Shi Pu, Yaole Wang, Gang Yue, Yue Cao, Hang Su, and Jun Zhu. One transformer fits all distributions in multi-modal diffusion at scale. 2023.

Tom Brown, Benjamin Mann, Nick Ryder, Melanie Subbiah, Jared D Kaplan, Prafulla Dhariwal, Arvind Neelakantan, Pranav Shyam, Girish Sastry, Amanda Askell, et al. Language models are few-shot learners. *Advances in neural information processing systems*, 33:1877–1901, 2020.

Prafulla Dhariwal and Alexander Nichol. Diffusion models beat gans on image synthesis. *Advances in neural information processing systems*, 34:8780–8794, 2021.

Jingtao Ding, Guanghui Yu, Yong Li, Depeng Jin, and Hui Gao. Learning from hometown and current city: Cross-city poi recommendation via interest drift and transfer learning. *Proceedings of the ACM on Interactive, Mobile, Wearable and Ubiquitous Technologies*, 3(4):1–28, 2019.

Yuntao Du, Jindong Wang, Wenjie Feng, Sinno Pan, Tao Qin, Renjun Xu, and Chongjun Wang. Adarnn: Adaptive learning and forecasting of time series. In *Proceedings of the 30th ACM international conference on information & knowledge management*, pp. 402–411, 2021.

Ziya Erkoç, Fangchang Ma, Qi Shan, Matthias Nießner, and Angela Dai. Hyperdiffusion: Generating implicit neural fields with weight-space diffusion. *arXiv preprint arXiv:2303.17015*, 2023.

Ziquan Fang, Dongen Wu, Lu Pan, et al. When transfer learning meets cross-city urban flow prediction: spatio-temporal adaptation matters. *IJCAI'22*, pp. 2030–2036, 2022.

Chelsea Finn, Pieter Abbeel, and Sergey Levine. Model-agnostic meta-learning for fast adaptation of deep networks. In *International conference on machine learning*, pp. 1126–1135. PMLR, 2017.

Leo Gao, Stella Biderman, Sid Black, Laurence Golding, Travis Hoppe, Charles Foster, Jason Phang, Horace He, Anish Thite, Noa Nabeshima, et al. The pile: An 800gb dataset of diverse text for language modeling. *arXiv preprint arXiv:2101.00027*, 2020.

Shansan Gong, Mukai Li, Jiangtao Feng, Zhiyong Wu, and Lingpeng Kong. Diffuseq: Sequence to sequence text generation with diffusion models. In *The Eleventh International Conference on Learning Representations*, 2022.

Ian Goodfellow, Jean Pouget-Abadie, Mehdi Mirza, Bing Xu, David Warde-Farley, Sherjil Ozair, Aaron Courville, and Yoshua Bengio. Generative adversarial networks. *Communications of the ACM*, 63(11):139–144, 2020.

Bin Guo, Jing Li, Vincent W Zheng, Zhu Wang, and Zhiwen Yu. Citytransfer: Transferring inter- and intra-city knowledge for chain store site recommendation based on multi-source urban data. *Proceedings of the ACM on Interactive, Mobile, Wearable and Ubiquitous Technologies*, 1(4): 1–23, 2018.

David Ha, Andrew M Dai, and Quoc V Le. "hypernetworks," in 5th international conference on learning representations, iclr 2017. In *Conference Track Proceedings, OpenReview. net*, pp. 24–26, 2017.

Kaiming He, Xinlei Chen, Saining Xie, Yanghao Li, Piotr Dollár, and Ross Girshick. Masked autoencoders are scalable vision learners. In *Proceedings of the IEEE/CVF conference on computer vision and pattern recognition*, pp. 16000–16009, 2022.

Tianfu He, Jie Bao, Ruiyuan Li, Sijie Ruan, Yanhua Li, Li Song, Hui He, and Yu Zheng. What is the human mobility in a new city: Transfer mobility knowledge across cities. In *Proceedings of The Web Conference 2020*, pp. 1355–1365, 2020.

Jonathan Ho, Ajay Jain, and Pieter Abbeel. Denoising diffusion probabilistic models. *Advances in neural information processing systems*, 33:6840–6851, 2020.

Jonathan Ho, William Chan, Chitwan Saharia, Jay Whang, Ruiqi Gao, Alexey Gritsenko, Diederik P Kingma, Ben Poole, Mohammad Norouzi, David J Fleet, et al. Imagen video: High definition video generation with diffusion models. *arXiv preprint arXiv:2210.02303*, 2022.

Yilun Jin, Kai Chen, and Qiang Yang. Selective cross-city transfer learning for traffic prediction via source city region re-weighting. In *Proceedings of the 28th ACM SIGKDD Conference on Knowledge Discovery and Data Mining*, pp. 731–741, 2022.

Xiang Li, John Thickstun, Ishaan Gulrajani, Percy S Liang, and Tatsunori B Hashimoto. Diffusion-lm improves controllable text generation. *Advances in Neural Information Processing Systems*, 35:4328–4343, 2022.

Yaguang Li, Rose Yu, Cyrus Shahabi, and Yan Liu. Diffusion convolutional recurrent neural network: Data-driven traffic forecasting. In *International Conference on Learning Representations*, 2018.

Zhonghang Li, Lianghao Xia, Yong Xu, and Chao Huang. Gpt-st: Generative pre-training of spatio-temporal graph neural networks. *arXiv preprint arXiv:2311.04245*, 2023.

Yan Liu, Bin Guo, Daqing Zhang, Djamal Zeghlache, Jingmin Chen, Ke Hu, Sizhe Zhang, Dan Zhou, and Zhiwen Yu. Knowledge transfer with weighted adversarial network for cold-start store site recommendation. *ACM Transactions on Knowledge Discovery from Data (TKDD)*, 15(3): 1–27, 2021.

Zhanyu Liu, Guanjie Zheng, and Yanwei Yu. Cross-city few-shot traffic forecasting via traffic pattern bank. *arXiv preprint arXiv:2308.09727*, 2023.

Zhaoyang Liu, Yanyan Shen, and Yanmin Zhu. Inferring dockless shared bike distribution in new cities. In *Proceedings of the eleventh ACM international conference on web search and data mining*, pp. 378–386, 2018.

Bin Lu, Xiaoying Gan, Weinan Zhang, Huaxiu Yao, Luoyi Fu, and Xinbing Wang. Spatio-temporal graph few-shot learning with cross-city knowledge transfer. In *Proceedings of the 28th ACM SIGKDD Conference on Knowledge Discovery and Data Mining*, pp. 1162–1172, 2022.

Zhengxiong Luo, Dayou Chen, Yingya Zhang, Yan Huang, Liang Wang, Yujun Shen, Deli Zhao, Jingren Zhou, and Tieniu Tan. Videofusion: Decomposed diffusion models for high-quality video generation. In *Proceedings of the IEEE/CVF Conference on Computer Vision and Pattern Recognition*, pp. 10209–10218, 2023.

Alexander Quinn Nichol and Prafulla Dhariwal. Improved denoising diffusion probabilistic models. In *International Conference on Machine Learning*, pp. 8162–8171. PMLR, 2021.

Alexander Quinn Nichol, Prafulla Dhariwal, Aditya Ramesh, Pranav Shyam, Pamela Mishkin, Bob Mcgrew, Ilya Sutskever, and Mark Chen. Glide: Towards photorealistic image generation and editing with text-guided diffusion models. In *ICML*, pp. 16784–16804. PMLR, 2022.

Zheyi Pan, Yuxuan Liang, Junbo Zhang, Xiuwen Yi, Yong Yu, and Yu Zheng. Hyperst-net: Hyper-networks for spatio-temporal forecasting. *arXiv preprint arXiv:1809.10889*, 2018.

Zheyi Pan, Yuxuan Liang, Weifeng Wang, Yong Yu, Yu Zheng, and Junbo Zhang. Urban traffic prediction from spatio-temporal data using deep meta learning. In *Proceedings of the 25th ACM SIGKDD international conference on knowledge discovery & data mining*, pp. 1720–1730, 2019.

Zheyi Pan, Wentao Zhang, Yuxuan Liang, Weinan Zhang, Yong Yu, Junbo Zhang, and Yu Zheng. Spatio-temporal meta learning for urban traffic prediction. *IEEE Transactions on Knowledge and Data Engineering*, 34(3):1462–1476, 2020.

Yanbo Pang, Kota Tsubouchi, Takahiro Yabe, and Yoshihide Sekimoto. Intercity simulation of human mobility at rare events via reinforcement learning. In *Proceedings of the 28th International Conference on Advances in Geographic Information Systems*, pp. 293–302, 2020.

William Peebles, Ilija Radosavovic, Tim Brooks, Alexei A Efros, and Jitendra Malik. Learning to learn with generative models of neural network checkpoints. *arXiv preprint arXiv:2209.12892*, 2022.

Robin Rombach, Andreas Blattmann, Dominik Lorenz, Patrick Esser, and Björn Ommer. High-resolution image synthesis with latent diffusion models. In *Proceedings of the IEEE/CVF conference on computer vision and pattern recognition*, pp. 10684–10695, 2022.

Chitwan Saharia, William Chan, Saurabh Saxena, Lala Li, Jay Whang, Emily L Denton, Kamyar Ghasemipour, Raphael Gontijo Lopes, Burcu Karagol Ayan, Tim Salimans, et al. Photorealistic text-to-image diffusion models with deep language understanding. *Advances in Neural Information Processing Systems*, 35:36479–36494, 2022.

Konstantin Schürholt, Dimche Kostadinov, and Damian Borth. Self-supervised representation learning on neural network weights for model characteristic prediction. *Advances in Neural Information Processing Systems*, 34:16481–16493, 2021.

Konstantin Schürholt, Boris Knyazev, Xavier Giró-i Nieto, and Damian Borth. Hyper-representations as generative models: Sampling unseen neural network weights. *Advances in Neural Information Processing Systems*, 35:27906–27920, 2022.

Zezhi Shao, Zhao Zhang, Fei Wang, Wei Wei, and Yongjun Xu. Spatial-temporal identity: A simple yet effective baseline for multivariate time series forecasting. In *Proceedings of the 31st ACM International Conference on Information & Knowledge Management*, pp. 4454–4458, 2022a.

Zezhi Shao, Zhao Zhang, Fei Wang, and Yongjun Xu. Pre-training enhanced spatial-temporal graph neural network for multivariate time series forecasting. In *KDD*, pp. 1567–1577, 2022b.

Jiaming Song, Chenlin Meng, and Stefano Ermon. Denoising diffusion implicit models. In *International Conference on Learning Representations*, 2020.

Yihong Tang, Ao Qu, Andy HF Chow, William HK Lam, SC Wong, and Wei Ma. Domain adversarial spatial-temporal network: a transferable framework for short-term traffic forecasting across cities. In *Proceedings of the 31st ACM International Conference on Information & Knowledge Management*, pp. 1905–1915, 2022.

Ashish Vaswani, Noam Shazeer, Niki Parmar, Jakob Uszkoreit, Llion Jones, Aidan N Gomez, Łukasz Kaiser, and Illia Polosukhin. Attention is all you need. *Advances in neural information processing systems*, 30, 2017.

Clément Vignac, Igor Krawczuk, Antoine Siraudin, Bohan Wang, Volkan Cevher, and Pascal Frossard. Digress: Discrete denoising diffusion for graph generation. In *Proceedings of the 11th International Conference on Learning Representations*, 2023.

Binwu Wang, Yudong Zhang, Xu Wang, Pengkun Wang, Zhengyang Zhou, Lei Bai, and Yang Wang. Pattern expansion and consolidation on evolving graphs for continual traffic prediction. In *Proceedings of the 29th ACM SIGKDD Conference on Knowledge Discovery and Data Mining*, pp. 2223–2232, 2023a.

Leye Wang, Xu Geng, Xiaojuan Ma, Feng Liu, and Qiang Yang. Cross-city transfer learning for deep spatio-temporal prediction. In *Proceedings of the 28th International Joint Conference on Artificial Intelligence*, pp. 1893–1899, 2019.

Xu Wang, Lianliang Chen, Hongbo Zhang, Pengkun Wang, Zhengyang Zhou, and Yang Wang. A multi-graph fusion based spatiotemporal dynamic learning framework. In *Proceedings of the Sixteenth ACM International Conference on Web Search and Data Mining*, pp. 294–302, 2023b.

Xu Wang, Pengfei Gu, Pengkun Wang, Binwu Wang, Zhengyang Zhou, Lei Bai, and Yang Wang. Graph-free learning in graph-structured data: A more efficient and accurate spatiotemporal learning perspective. *arXiv preprint arXiv:2301.11742*, 2023c.

Ying Wei, Yu Zheng, and Qiang Yang. Transfer knowledge between cities. In *Proceedings of the 22nd ACM SIGKDD International Conference on Knowledge Discovery and Data Mining*, pp. 1905–1914, 2016.

Haomin Wen, Youfang Lin, Yutong Xia, Huaiyu Wan, Qingsong Wen, Roger Zimmermann, and Yuxuan Liang. Diffstg: Probabilistic spatio-temporal graph forecasting with denoising diffusion models. In *Proceedings of the 31st ACM International Conference on Advances in Geographic Information Systems*, pp. 1–12, 2023.

Zonghan Wu, Shirui Pan, Guodong Long, Jing Jiang, and Chengqi Zhang. Graph wavenet for deep spatial-temporal graph modeling. *arXiv preprint arXiv:1906.00121*, 2019.

Yutong Xia, Yuxuan Liang, Haomin Wen, Xu Liu, Kun Wang, Zhengyang Zhou, and Roger Zimmermann. Deciphering spatio-temporal graph forecasting: A causal lens and treatment. *Advances in Neural Information Processing Systems*, 36, 2024.

Huaxiu Yao, Yiding Liu, Ying Wei, Xianfeng Tang, and Zhenhui Li. Learning from multiple cities: A meta-learning approach for spatial-temporal prediction. In *WWW*, pp. 2181–2191, 2019.

Bing Yu, Haoteng Yin, and Zhanxing Zhu. Spatio-temporal graph convolutional networks: A deep learning framework for traffic forecasting. *arXiv preprint arXiv:1709.04875*, 2017.

Yuan Yuan, Jingtao Ding, Chenyang Shao, Depeng Jin, and Yong Li. Spatio-temporal diffusion point processes. In *Proceedings of the 29th ACM SIGKDD Conference on Knowledge Discovery and Data Mining*, pp. 3173–3184, 2023.

Zhengyang Zhou, Qihe Huang, Kuo Yang, Kun Wang, Xu Wang, and Yudong Zhang. Maintaining the status quo: Capturing invariant relations for ood spatiotemporal learning. 2023a.

Zhengyang Zhou, Jiahao Shi, Hongbo Zhang, Qiongyu Chen, Xu Wang, Hongyang Chen, and Yang Wang. Crest: A credible spatiotemporal learning framework for uncertainty-aware traffic forecasting. In *The 17th ACM International Conference on Web Search and Data Mining*, pp. 1–10, 2024.

Zhilun Zhou, Jingtao Ding, Yu Liu, Depeng Jin, and Yong Li. Towards generative modeling of urban flow through knowledge-enhanced denoising diffusion. *arXiv preprint arXiv:2309.10547*, 2023b.

Fuzhen Zhuang, Zhiyuan Qi, Keyu Duan, Dongbo Xi, Yongchun Zhu, Hengshu Zhu, Hui Xiong, and Qing He. A comprehensive survey on transfer learning. *Proceedings of the IEEE*, 109(1): 43–76, 2020.
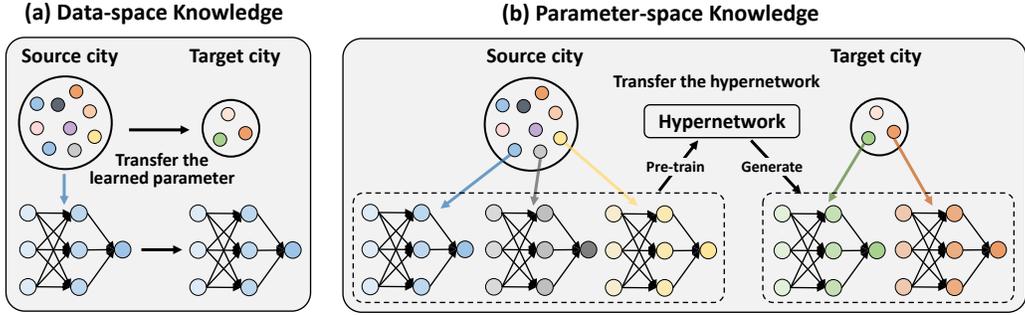
Figure 5: Comparison of data-space and parameter-space knowledge across cities. Colorful points represent divided regions in the city.

A   METHODOLOGY DETAILS

A.1   DIFFERENT KNOWLEDGE FOR TRANSFER

Figure 5 compares the difference between our framework and other urban transfer learning methods, which focus on parameter-space knowledge and data-space knowledge, respectively.

A.2   REGION PROMPTS

We design region prompts to leverage auxiliary data that captures city characteristics. This prompting technique facilitates to utilize external information more flexibly. In our experiments, we adopt a granular approach by crafting distinct prompts for each region within the city. These prompts are meticulously designed to encapsulate the unique characteristics of each region. To facilitate accurate spatio-temporal predictions, we create two specific types of prompts: a spatial prompt and a temporal prompt. The spatial prompt is tailored to provide an in-depth representation of the spatial attributes, encompassing geographical features, environmental conditions, and interconnections with neighboring regions. Complementing the spatial prompt, we also introduce a temporal prompt. This prompt captures the temporal dynamics of each region.

Spatial Prompt.   The spatial prompt is obtained by pre-training an urban knowledge graph (UKG) (Zhou et al., 2023b), which is meticulously designed to encapsulate the extensive environmental information within a city. Specifically, we represent urban regions as distinct entities within the UKG framework. We use relations "BorderBy" and "NearBy" to capture the spatial adjacency among regions. By leveraging this adjacency representation, we aim to capture the influence that proximate regions exert on one another. Furthermore, our UKG incorporates an understanding of the functional similarity between these urban regions. This insight is quantified by computing the cosine similarity of the distribution of Points of Interest (POI) categories between region pairs. We establish a "SimilarFunc" relation to establish connections between regions that exhibit functional similarity, which emphasizes the critical role played by shared functions in shaping the urban landscape.

Relation	Head & Tail Entity Types	Semantic Information
BorderBy	(Region, Region)	Regions share part of the boundary
NearBy	(Region, Region)	Regions are within a certain distance
SimilarFunc	(Region, Region)	Regions have similar functions

Table 3: The details of relations in the urban knowledge graph.

To extract the spatial prompts from the constructed Urban Knowledge Graph (UKG), we employ a state-of-the-art KG embedding model, TuckER (Balažević et al., 2019), to learn an embedding representation for each region. TuckER evaluates the plausibility of triplets as follows:

$$\phi(h, r, t) = \mathcal{W} \times_1 e_h \times_2 e_r \times_3 e_t, \tag{3}$$

14

where $\mathcal{W} \in \mathbb{R}^{d_{KG}^3}$ is a learnable tensor, $\times_n$ denotes the tensor product along the n_{th} dimension, and $e_h, e_r, e_t \in \mathbb{R}_{KG}^d$ are the embeddings of head entity h, tail entity t and relation r respectively. The primary objective of the KG embedding model is to maximize the scoring function for triplets that exist in the UKG, thereby preserving the knowledge contained within the UKG.

In summary, our UKG leverages the 'BorderBy' and 'NearBy' relationships to articulate spatial connections and the 'SimilarFunc' relationship to underscore functional parallels between urban regions. The benefits of UKG are twofold. First, it integrates various relationships within the city, allowing the learned embeddings of regions to provide descriptive information about their respective urban environments. Secondly, in contrast to time series data collected by sensors or GPS devices, the features utilized in the Urban Knowledge Graph (UKG) are readily available in all urban areas. This accessibility makes the UKG scalable and adaptable to cities, even those with limited development levels. The details of relations in UKG are shown in Table 3.

Temporal Prompt. The temporal prompt is derived through a strategic application of an unsupervised pre-training model designed for time series, as introduced by Shao et al (Shao et al., 2022b). This approach shares similarities with the concept of a Masked AutoEncoder (MAE) (He et al., 2022) for sequence data. Initially, the time series data for each region is subjected to a masking procedure, where random patches within the time series are concealed. Subsequently, an encoder-decoder model is trained on this modified data to reconstruct the original time series. This training process is centered around the objective of reconstructing the complete time series based solely on the partially observable series patches. Given that time series data often exhibits lower information density, a relatively high masking ratio (75%) is employed. This higher masking ratio is crucial for creating a self-supervised learning challenge that encourages the model to capture meaningful temporal patterns from incomplete observations. Upon successful completion of the self-supervised learning phase for time series data, the output of the encoder yields the temporal embeddings. In essence, this method capitalizes on self-supervised learning to extract valuable temporal features from time series data, which can subsequently be used as temporal prompts.

A.3 CONDITIONING STRATEGIES

Pre-conditioning. "Pre" denotes that the prompt is integrated into the token sequence before being fed into self-attention layers. In this method, we simply add the region prompt p to the token embeddings within the input sequence.

Pre-conditioning with inductive bias. In this variant, we adopt a different approach to add the region prompt p to the token embeddings within the input sequence. The spatial prompt is incorporated into spatial-related parameters uniformly and the temporal prompt into temporal-related parameters uniformly as follows:

$$[\boldsymbol{x}_{s,1}, \boldsymbol{x}_{s,1}, \cdots, \boldsymbol{x}_{s,m}] = [\boldsymbol{x}_{s,1}, \boldsymbol{x}_{s,1}, \cdots, \boldsymbol{x}_{s,m}] + \underbrace{[\boldsymbol{p}_s, \boldsymbol{p}_s, \cdots, \boldsymbol{p}_s]}_{m}$$

$$[\boldsymbol{x}_{t,1}, \boldsymbol{x}_{t,1}, \cdots, \boldsymbol{x}_{t,n}] = [\boldsymbol{x}_{t,1}, \boldsymbol{x}_{t,1}, \cdots, \boldsymbol{x}_{t,n}] + \underbrace{[\boldsymbol{p}_t, \boldsymbol{p}_t, \cdots, \boldsymbol{p}_t]}_{n}, \tag{4}$$

where m and n represent the number of tokens for spatial parameters and temporal parameters, p_s denotes the spatial prompt, and p_t denotes the temporal prompt.

Pre-adaptive conditioning. In this variant, we introduce an attention mechanism, which determines to what extent the prompt should be added to specific token embeddings. We denote the prompt as $p \in \mathbb{R}^{2 \times E}$, where E is the embedding size of spatial and temporal prompts. This approach aims to empower the model to learn how to adaptively utilize the prompts, enhancing its conditioning capabilities. The utilization of the prompt can be formulated as follows:
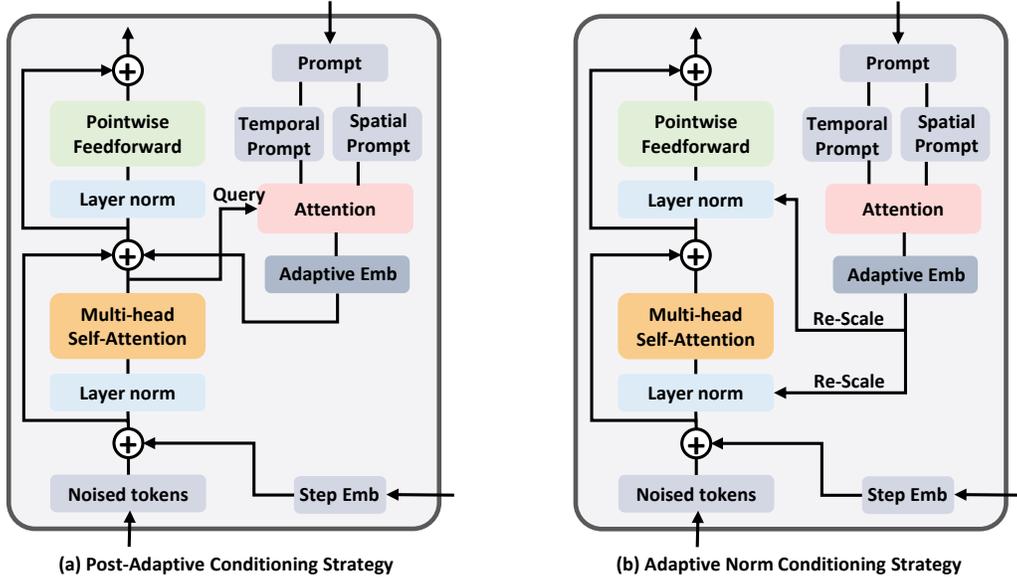
Figure 6: Illustration of two conditioning strategies: (a) "Post-Adaptive Conditioning" and (b) "Adaptive Norm Conditioning".

$$u_j = \tanh(W_w p_j + b_w), j \in \{0, 1\} \tag{5}$$

$$\alpha_{i,j} = \frac{\exp(u_j^T, x_i)}{\sum_k \exp(u_k^T, x_i)} \tag{6}$$

$$P_i = \sum_j \alpha_{i,j} p_j, j \in \{0, 1\} \tag{7}$$

where p_0 and p_1 represent the spatial prompt and temporal prompt, respectively, P_i denotes the aggregated prompt from two aspects for the i_{th} token.

Post-adaptive Conditioning. Figure 6 (a) illustrates this conditioning strategy. The aggregated prompt based on the attention mechanism is added after the multi-head self-attention in each transformer layer. Specifically, the query used for spatio-temporal attentive aggregation is the output of the multi-head self-attention layer.

Adaptive norm conditioning. Figure 6 (b) illustrates this conditioning strategy. The aggregated prompt based on the attention mechanism is used for re-scaling the output in each layer norm.

A.4 NETWORK LAYERS OF SPATIO-TEMPORAL PREDICTION MODELS

We provide details of parameter tokenizers introduced in Section 3.5. In our experiments, we implement our framework on three spatio-temporal prediction models, STGCN (Yu et al., 2017), GWN (Wu et al., 2019), and STID (Shao et al., 2022a). We present how to transform their network layers into a vector-based token sequence. According to Table 4 and Table 5, the transformation from parameter layers to a token sequence can be formulated as follows:

$$
\begin{aligned}
gcd &= GCD(numel(s_1), numel(s_2), \ldots, numel(s_m)) \\
L_i &= c_i * numel(s_i)/gcd \\
L &= \sum_i L_i,
\end{aligned}
\tag{8}
$$

where GCD denotes the calculation of the Greatest Common Divisor, m denotes the number of different layer types, s_i denotes the shape, $numel$ denotes the total number of elements in the tensor

	Layer name	Parameter shape	Count
	Block1-TimeBlock1-conv	[32,2,1,4]	3
Block1	Block1-GraphConv_Theta1	[32,8]	1
	Block1-TimeBlock2-conv	[32,8,1,4]	3
TimeBlock	last_TimeBlock-conv	[32,32,1,4]	3
Linear	Fully Connected Layer	[6,96]	1

Table 4: Parameter structure of a STGCN Model

Layer name	Parameter shape	Count
filter_convs.x	$[32, 32, 1, 2]$	8
gate_convs.x	$[32, 32, 1, 2]$	8
residual_convs.x	$[32, 32, 1, 1]$	8
skip_convs.x	$[32, 32, 1, 1]$	8
bn.x	$[32] + [32]$	8
gconv.x.mlp.mlp	$[32, 160, 1, 1]$	8
start_conv	$[32, 2, 1, 1]$	1
end_conv1	$[32, 32, 1, 1]$	1
end_conv2	$[6, 32, 1, 1]$	1

Table 5: Parameter structure of a GWN Model

	Layer name	Parameter shape	Count
Time_series_emb	conv	[32,24,1,1]+[32]	1
	Layer1-fc	[32,32,1,1]+[32]	2
EncoderLayers	Layer2-fc	[32,32,1,1]+[32]	2
	Layer3-fc	[32,32,1,1]+[32]	2
Regression_layer	conv	[6,32,1,1]	1

Table 6: Parameter structure of a STID Model

c_i denotes the count of this type of layer. In this way, we obtain a token sequence with length as L and embedding size as gcd.

STGCN (Yu et al., 2017). Spatio-temporal graph convolution network. Different from regular convolutional and recurrent units, this model build convolutional structures on graphs. We use a 3-layer STGCN block, and utilize a 1-layer MLP as the output predictor. Table 4 shows the detailed network layers of a STGCN.

GWN (Wu et al., 2019). Graph WaveNet. This model developed a novel adaptive dependency matrix and learned it through node embeddings to capture the spatial dependency. It also combines with a stacked dilated causal convolution component. We use a 2-layer 4-block GWN model. Table 4 shows the detailed network layers of a GWN.

STID (Shao et al., 2022a). Spatio-Temporal Identity. This model is a simple Multi-Layer Perceptrons (MLPs)-based approach. By identifying the indistinguishability of samples in both spatial and temporal dimensions, it is simple yet effective for spatio-temporal prediction.

A.5 ALGORITHMS

We present the training algorithm for spatio-temporal graph prediction in Algorithm 1. Besides, we present the training algorithm and sampling algorithm for the diffusion model in Algorithm 2 and Algorithm 3, respectively.

B EXPERIMENT DETAILS

B.1 DATASETS

In this section, we introduce the details of the used real-world datasets.

Algorithm 1 Model Parameter Preparation

1: **Input**: Dataset $D = \{D_1, D_2, \ldots, D_{M_s}\}$, neural networks $F = \{f_{\theta_1}, f_{\theta_2}, \ldots, f_{\theta_{M_s}}\}$ of the spatio-temporal prediction model, loss function L, parameter storage S.
2: **Output**: Parameter storage S.
3: **Initialize**: Learnable parameters θ_m for f_m, parameter storage $S = \{\}$.
4: **for** $m \in \{1, 2, \ldots, M_s\}$ **do**
5:      **for** $epoch \in \{1, 2, \ldots, N_{iter}\}$ **do**
6:          Sample a mini-batch of inputs and labels from the dataset D_m $\{x, y\} \sim D_m$
7:          Compute the predictions $\hat{y} \leftarrow f_{\theta_m}(x)$
8:          Compute the loss $\mathcal{L} \leftarrow L(\hat{y}, y)$
9:          Update the model's parameters $\theta_m \leftarrow update(\mathcal{L}; \theta_m)$
10:      **end for**
11:      Save the optimized model $S \leftarrow S \cup \{\theta_m\}$
12: **end for**

Algorithm 2 Generative Pre-training of the Diffusion Model

1: **Input**: Parameter storage S, diffusion model G.
2: **Initialize**: Learnable parameters γ for G
3: **for** $epoch \in \{1, 2, \ldots, N_{iter}\}$ **do**
4:      Sample a parameter sample $\theta_0 \sim q(\theta_0)$ and $\epsilon \sim \mathcal{N}(0, I)$
5:      Sample diffusion step $k \sim \text{Uniform}(1, \ldots, K)$
6:      Take gradient descent step on

$$\nabla_\gamma \|\epsilon - \epsilon_\gamma(\sqrt{\overline{\alpha}_k}\theta_0 + \sqrt{1 - \overline{\alpha}_k}\epsilon, p, k)\|^2$$

7: **end for**

Algorithm 3 Parameter Sampling

1: **Input**: Gaussian noise $\theta_K \sim \mathcal{N}(0, I)$, prompts $P = \{p_1, p_2, \ldots, M\}$
2: **Output**: Parameters $\theta_t = \{\theta_{1,0}, \theta_{2,0}, \ldots, \theta_{M_t,0}\}$.
3: **Initialize**: Learnable parameters γ for G, $\theta_s = \{\}$.
4: **for** $m \in \{1, 2, \ldots, M_t\}$ **do**
5:      **for** $k = K \rightarrow 1$ **do**
6:          **if** $K > 1$ **then**
7:              $z \sim \mathcal{N}(0, I)$
8:          **else**
9:              $z = 0$
10:          **end if**
11:

$$\theta_{m,k-1} = \frac{1}{\sqrt{\alpha_k}}\left(\theta_{m,k} - \frac{\beta_k}{\sqrt{1 - \overline{\alpha}_k}}\epsilon_\gamma(\theta_{m,k}, p, k)\right) + \sqrt{\beta_k}z$$

12:      **end for**
13:      $\theta_s = \theta_s \cup \theta_{m,0}$
14: **end for**

Datasets	New York City	Washington, D.C.	Baltimore
#Nodes	195	194	267
#Edges	555	504	644
Interval	1 hour	1 hour	1 hour
Time span	2016.01.01-2016.06.30	2019.01.01-2019.05.31	2019.01.01-2019.05.31
Mean	70.066	30.871	18.763
Std	71.852	58.953	28.727

Table 7: The basic information and statistics of four real-world datasets for crowd flow prediction.

Datasets	METR-LA	PEMS-BAY	Didi-Chengdu	Didi-Shenzhen
#Nodes	207	325	524	627
#Edges	1722	2694	1120	4845
Interval	5 min	5 min	10 min	10 min
Time span	2012.05.01-2012.06.30	2017.01.1-2017.06.30	2018.1.1-2018.4.30	2018.1.1-2018.4.30
Mean	58.274	61.776	29.023	31.001
Std	13.128	9.285	9.662	10.969

Table 8: The basic information and statistics of four real-world datasets for traffic speed prediction.

B.1.1 CROWD FLOW PREDICTION.

- **NYC Dataset.** In this dataset, we define regions as census tracts and aggregate taxi trips from NYC Open Data to derive hourly inflow and outflow information. The division of train and test regions is based on community districts. Specifically, the Manhattan borough comprises 12 community districts, and we designate 9 of them as train regions, reserving the remaining 3 for testing. Region-specific features encompass the count of Points of Interest (POIs), area, and population.

- **Washington, D.C. Dataset.** Regions in this dataset are defined as census tracts, and inflow data is calculated based on Point of Interest (POI)-level hourly visits. The partitioning of train and test regions is done by counties. Specifically, regions within the District of Columbia are selected as train regions, and regions in Arlington County are designated as test regions. This dataset comprises rich region features, including demographics and socioeconomic indicators.

- **Baltimore Dataset.** Similar to the D.C. dataset, regions, and inflow data in the Baltimore dataset are obtained in the same manner. Train regions consist of regions in Baltimore City, while test regions encompass Baltimore County. This dataset includes the same set of features as the D.C. dataset.

B.1.2 TRAFFIC SPEED PREDICTION.

We conducted our performance evaluation using four real-world traffic speed datasets, following the data preprocessing procedures established in prior literature (Li et al., 2018; Lu et al., 2022). To construct the spatio-temporal graph, we treated each traffic sensor or road segment as an individual vertex within the graph. We then computed pairwise road network distances between these sensors. Finally, we construct the adjacency matrix of the nodes using road network distances and a thresholded Gaussian kernel.

- **METR-LA (Li et al., 2018; Lu et al., 2022).** The traffic data in our study were obtained from observation sensors situated along the highways of Los Angeles County. We utilized a total of 207 sensors, and the dataset covered a span of four months, ranging from March 1, 2012, to June 30, 2012. To facilitate our analysis, the sensor readings were aggregated into 5-minute intervals.

- **PEMS-BAY (Li et al., 2018; Lu et al., 2022).** The PEMS-BAY dataset comprises traffic data collected over a period of six months, from January 1st, 2017, to June 30th, 2017, within the Bay Area. The dataset is composed of records from 325 traffic sensors strategically positioned throughout the region.

- **Didi-Chengdu (Lu et al., 2022).** We utilized the Traffic Index dataset for Chengdu, China, which was generously provided by the Didi Chuxing GAIA Initiative. Our dataset selection encompassed the period from January to April 2018 and covered 524 roads situated within the central urban area of Chengdu. The data was collected at 10-minute intervals to facilitate our analysis.
- **Didi-Shenzhen (Lu et al., 2022).** We utilized the Traffic Index dataset for Shenzhen, China, which was generously provided by the Didi Chuxing GAIA Initiative. Our dataset selection included data from January to April 2018 and encompassed 627 roads located in the downtown area of Shenzhen. The data collection was conducted at 10-minute intervals to facilitate our analysis.

B.2 BASELINES

- **HA.** Historical average approach models time series as a seasonal process and leverages the average of previous seasons for predictions. In this method, we utilize a limited set of target city data to compute the daily average value for each node. This historical average then serves as the baseline for predicting future values.
- **ARIMA.** Auto-regressive Integrated Moving Average model is a widely recognized method for comprehending and forecasting future values within a time series.
- **RegionTrans (Wang et al., 2019).** RegionTrans assesses the similarity between source and target nodes, employing it as a means to regulate the fine-tuning of the target. We use STGCN and GWN as its base model.
- **DASTNet (Tang et al., 2022).** Domain Adversarial Spatial-Temporal Network, which undergoes pre-training on data from multiple source networks and then proceeds to fine-tune using the data specific to the target network's traffic.
- **AdaRNN (Du et al., 2021).** This cutting-edge transfer learning framework is designed for non-stationary time series data. The primary objective of this model is to mitigate the distribution disparity within time series data, enabling the training of an adaptive model based on recurrent neural networks (RNNs).
- **MAML (Finn et al., 2017).** Model-Agnostic Meta Learning is an advanced meta-learning technique designed to train a model's parameters in a way that a minimal number of gradient updates result in rapid learning on a novel task. MAML achieves this by acquiring an improved initialization model through the utilization of multiple tasks to guide the learning process of the target task.
- **TPB (Liu et al., 2023).** Traffic Pattern Bank-based approach. TPB employs a pre-trained traffic patch encoder to transform raw traffic data from cities with rich data into a high-dimensional space. In this space, a traffic pattern bank is established through clustering. Subsequently, the traffic data originating from cities with limited data availability can access and interact with the traffic pattern bank to establish explicit relationships between them.
- **ST-GFSL (Lu et al., 2022).** ST-GFSL generates node-specific parameters based on node-level meta-knowledge drawn from the graph-based traffic data. This approach ensures that parameters are tailored to individual nodes, promoting parameter similarity among nodes that exhibit similarity in the traffic data.

B.3 IMPLEMENTATION DETAILS

In the experiments, we set the number of diffusion steps N=500. The learning rate is set to 8e-5 and the number of training epochs ranges from 3000 to 12000. The dimensions of KG embedding and time embedding are both 128. Regarding the spatio-temporal prediction, we use 12 historical time steps to predict 6 future time steps. Our framework can be effectively trained within 3 hours and all experiments were completed on one NVIDIA GeForce RTX 4090.

C ADDITIONAL RESULTS

C.1 FLEXIBILITY OF GPD

To demonstrate the flexibility of our framework, we compare the performance with GWN as the base model. Figure 8 to Figure 10 illustrate the comparison results. As we can observe, our frame-

work still achieves the best performance on all datasets. The advantage of our framework is more significant for long-step predictions.
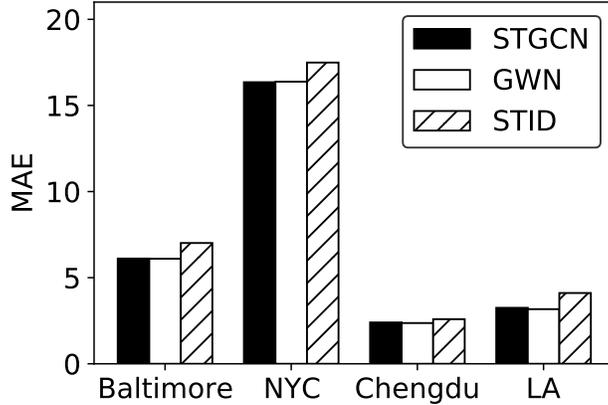
Figure 7: Performance comparison of different spatio-temporal prediction models on crowd flow prediction task (Baltimore and NYC) and traffic speed prediction task (Chengdu and LA).
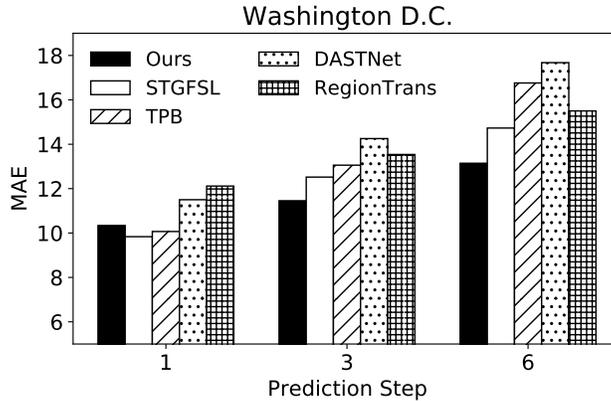
Figure 8: Performance comparison with GWN as the base model on Washington D.C. dataset.

C.2 TIME CONSUMPTION ANALYSIS

Model	RegionTrans	DASTNet	MAML	TPB	STGFSL	GPD
Computational cost	~1.5min	~1h	~2h	~1h	~2h	~3h

Table 9: Training time consumption of our framework and baseline solutions.

Table 9 present a detailed comparison of the computational cost of our proposed model against baselines. Our model demonstrates efficient training, completing within 3 hours on a single GPU (RTX-2080Ti), which we believe is an acceptable time consumption. It is important to note that the slightly longer time consumption in our model is attributed to the step-by-step denoising process implemented in DDPM approach (Ho et al., 2020).

We choose DDPM because it is a classic, simple but effective diffusion framework. Notably, our framework is designed to be compatible with more efficient diffusion models, such as DDIM (Song et al., 2020). Employing these models has the potential to significantly reduce the current computational cost. We want to underscore that our framework has the ability to achieve remarkably better performance with a relatively lower overhead.
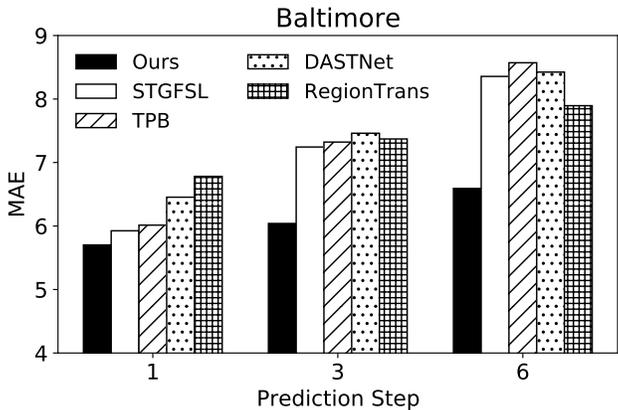
Figure 9: Performance comparison with GWN as the base model on Baltimore dataset.
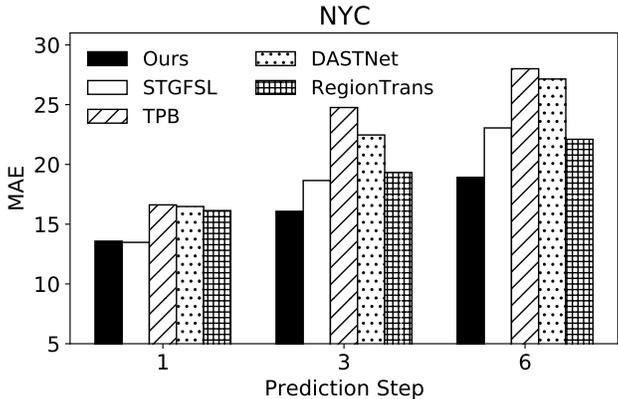
Figure 10: Performance comparison with GWN as the base model on NYC dataset.

C.3 FINE-GRAINED PERFORMANCE ANALYSIS

We conducted fine-grained evaluations to discern the types of regions in target cities that benefit more from knowledge transfer in our pretraining framework. For this analysis, we selected Baltimore as the target city, while Washington D.C. and NYC served as source cities. To initiate our investigation, we analyzed the performance differences across various regions within Baltimore. The distribution of performance across these regions is visualized in Figure 11. This observation of varied performance across different regions prompted us to explore the factors contributing to this performance variance, aiming to gain insights into more effective knowledge transfer strategies.

In our analysis, we employed clustering on the time series data from the source cities. Figure 12 provides a visual representation of the time series data through Principal Component Analysis (PCA). Simultaneously, we conducted an in-depth analysis focusing on regions within the target city. Specifically, we selected two regions with relatively superior performance (MAE = 2.53 and 2.33) and two regions with comparatively lower performance (MAE = 30.2, 31.8). As illustrated in Figure 12, regions with better performance (depicted in red as the "good case") seamlessly align with one of the clusters identified in the source cities. In contrast, regions with lower performance (depicted in blue as the "bad case") are situated farther from the clustering centers, struggling to align with any specific clusters. This insightful observation aligns with the intuitive notion that regions sharing similar patterns are more receptive to knowledge transfer within our pretraining framework. Consequently, leveraging more diverse cities as source cities for pretraining the generative framework promises to improve overall performance. This insight is consistent with the principles observed

in Large Language Models, which often exhibit enhanced performance when trained on a highly diverse dataset (Gao et al., 2020).
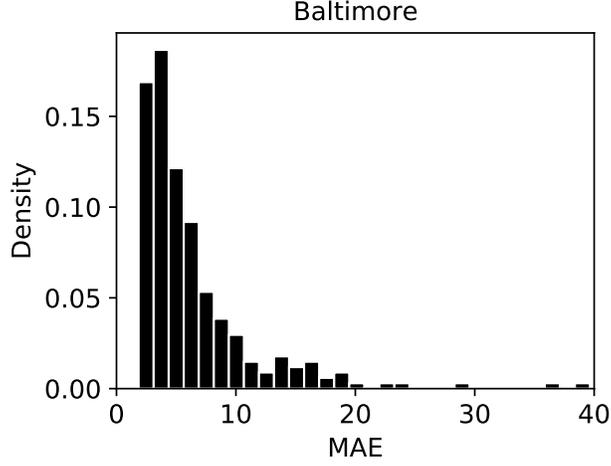
Figure 11: Performance distribution of different regions in Baltimore.
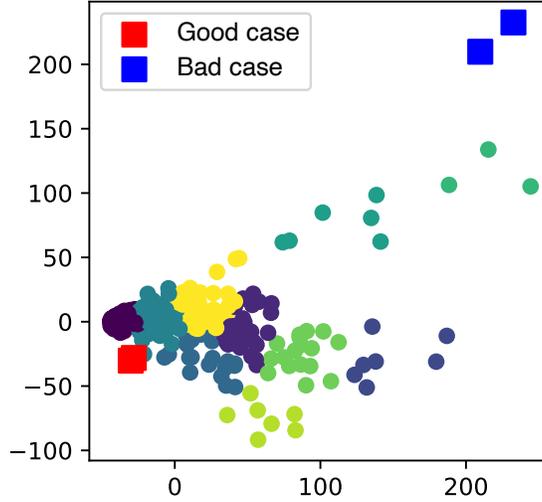
Figure 12: Clustering visualization of the source city data and the case study of the target city.

C.4 SYNTHETIC DATA EXPERIMENTS

The effectiveness of our approach is grounded in two key hypotheses:

Assumption 1. *Regions with distinct spatio-temporal patterns correspond to different optimized model parameters. This relationship can be mathematically expressed as follows:*

$$P_i^* \neq P_j^* \quad if \quad D(X_i, X_j) > \epsilon, \tag{9}$$

where P_i^* represents the optimized model parameters for region i, X_i denotes the spatio-temporal pattern of the region i, D signifies the dissimilarity metric between the patterns of two regions.

Assumption 2. *There exists a mapping relation f_θ between the conditions from each region C_i and the optimized model parameters P_i^*.*

$$P_i = f_\theta(C_i) \quad where \quad \theta = \underset{\theta}{argmin} \sum_i Distance(P_i^*, f_\theta(X_i)) \tag{10}$$

23
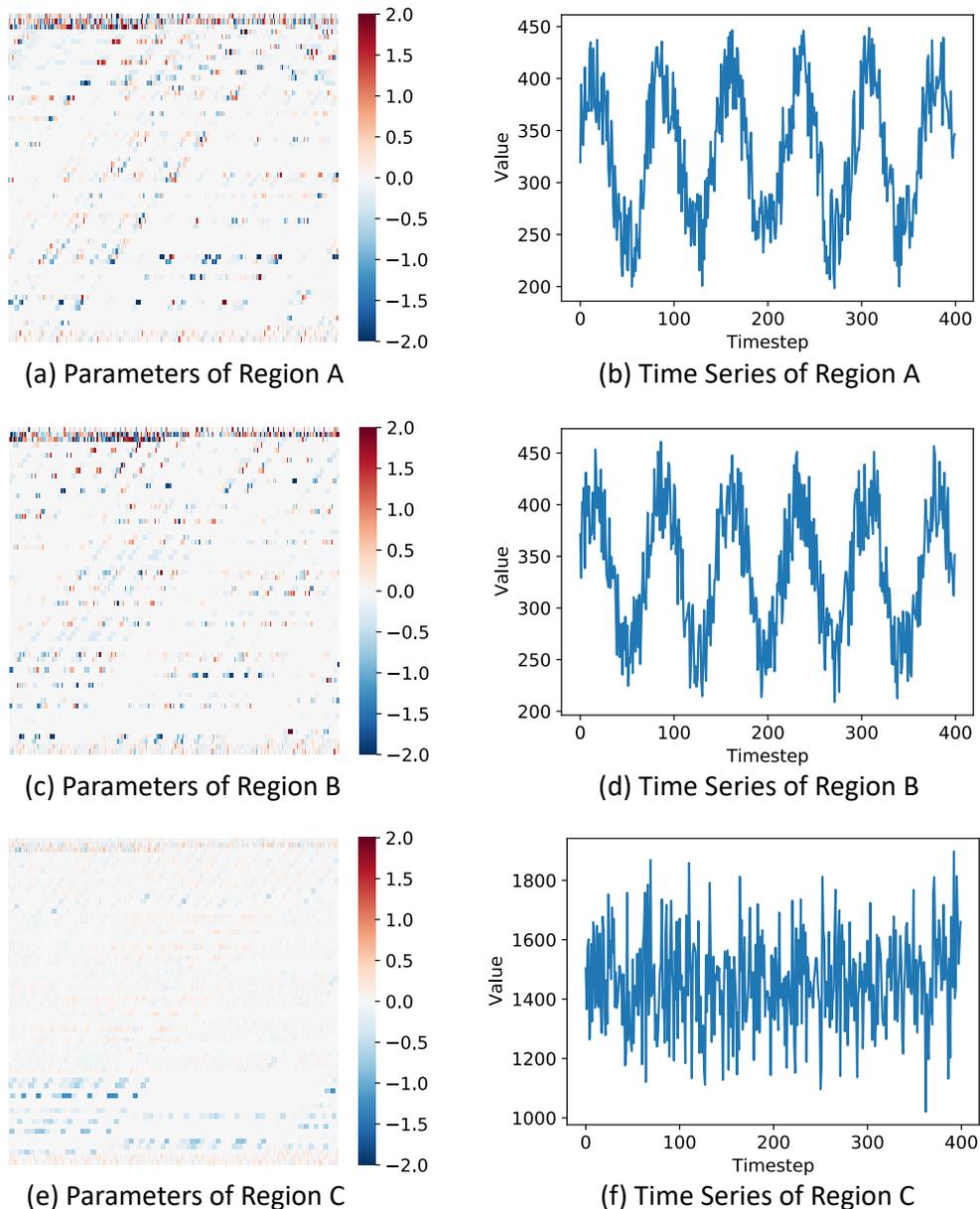
Figure 13: Visualization of parameters and time series for three regions in the source city.

where P_i is the generated model parameters.

To empirically validate these hypotheses, we conducted experiments on two synthetic datasets, allowing us to manipulate pattern similarities between nodes. This design enables an investigation into the framework's ability to generate effective parameters. The experimental setup involves two cities: one designated as the source city, and the other as the target city, each comprising 200 regions. We first construct a graph by randomly adding edges between regions. Then, for each region, we generated a time series following specific patterns while incorporating random noise. This approach ensured that regions have distinct spatio-temporal patterns.

In Figure 13, we present the parameter maps of well-trained models for three regions in the source city. Notably, regions A (Figure 13(b)) and B (Figure 13(d)) exhibit highly similar time series patterns, whereas region C (Figure 13(f)) displays distinctly different patterns. In the meantime, the

(a) Ground-truth Parameters of Region M (b) Generated Parameters of Region M

(d) Ground-truth Parameters of Region N (d) Generated Parameters of Region N
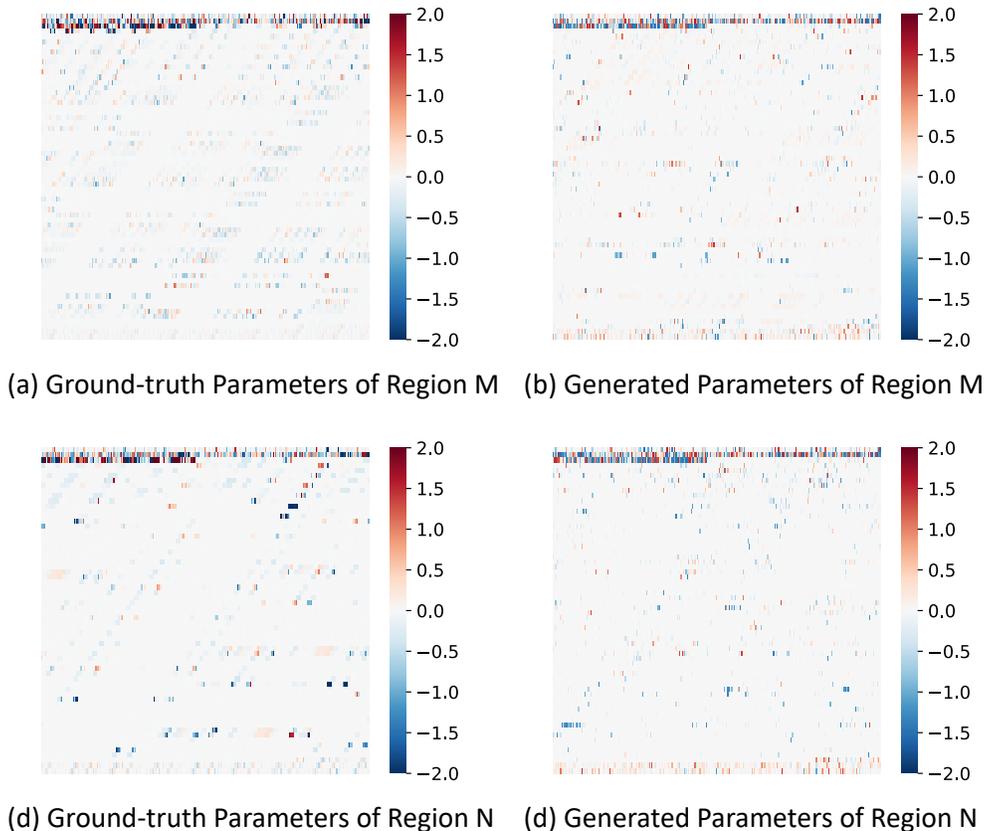
Figure 14: Visualization of ground-truth parameters and generated parameters for two regions in the target city.

symmetrical positions of nodes A and B in the graph (depicted in Figure 15) suggest that regions A and B have very similar spatial patterns. Therefore, we can assume that regions A and B have very similar spatio-temporal patterns. Consequently, the parameter maps for regions A and B showcase similar distributions, diverging from the parameter map of region C. This observation underscores the necessity of employing non-shared parameters for regions to effectively adapt to diverse spatio-temporal patterns.

Moving on to the parameter generation results for the target city, we selected two regions labeled as M and N, characterized by similar time series patterns and spatial connection locations (see Figure 16). Figure 14 illustrates the comparison results. Specifically, Figures 14(a) and 14(c) depict the ground truth parameter maps for these two regions, revealing similar distribution patterns. Figures 14(b) and 14(d) illustrate the generated parameter maps for the same regions. Notably, the generated parameter maps closely align with their corresponding ground-truth distributions. This comprehensive analysis of parameter generation, presented in Figures 13, Figures 14, Figure 15, and Figure 16, collectively validates the capability of our framework in effectively generating parameters that capture diverse spatio-temporal patterns across different regions.

C.5   PREDICTION RESULTS OF THE REMAINING CITIES

Table 10 to Table 14 show the prediction results of other datasets.
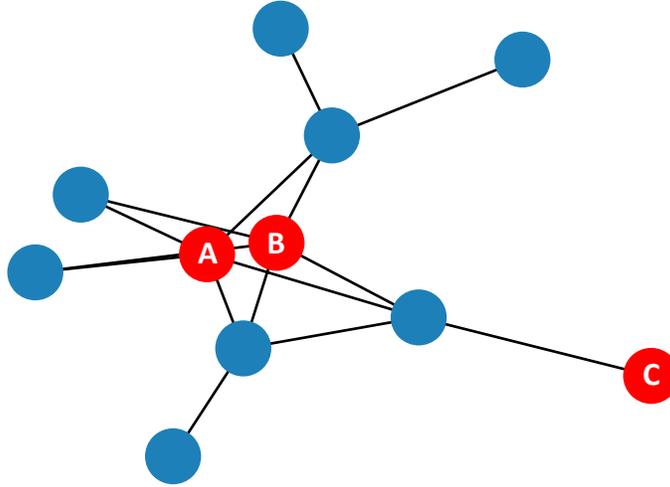
Figure 15: The sub-graph of the source city, which contains nodes A, B, and C. The graph structure denotes spatial connection relationships.
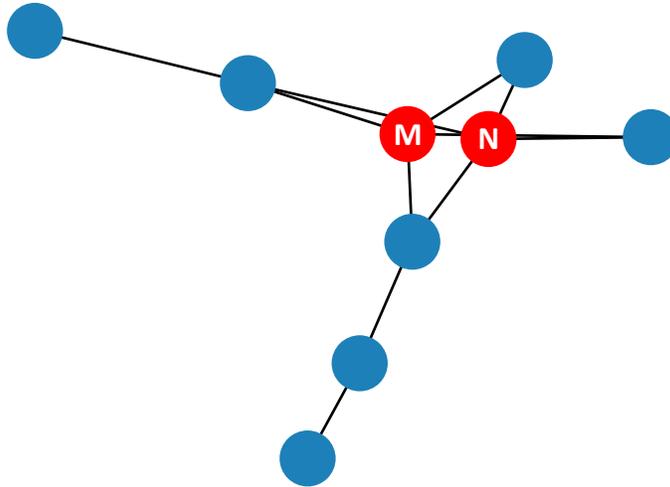
Figure 16: The sub-graph of the target, which contains nodes M and N.

	MAE			RMSE		
Model	Step 1	Step 3	Step 6	Step 1	Step 3	Step 6
HA	21.520	21.520	21.520	47.122	47.122	47.122
ARIMA	19.703	15.063	27.083	37.809	35.093	61.675
RegionTrans	12.116	13.538	15.501	27.622	30.999	36.095
DASTNet	11.501	14.255	17.676	25.551	31.466	38.004
MAML	10.831	13.634	16.192	24.455	30.740	36.271
TPB	**9.153**	_11.870_	15.236	23.420	28.756	33.424
STGFSL	9.636	12.178	_14.116_	**22.362**	_28.287_	_33.547_
GPD	_10.339_	**11.454**	**13.144**	_23.348_	**26.798**	**30.959**

Table 10: Performance comparison of few-shot scenarios on Washington D.C. dataset at different prediction steps in terms of MAE and RMSE. Bold denotes the best results and underline denotes the second-best results.

	MAE			RMSE		
Model	Step 1	Step 3	Step 6	Step 1	Step 3	Step 6
HA	15.082	15.082	15.082	26.768	26.768	26.768
ARIMA	11.150	12.344	18.557	19.627	21.665	35.520
RegionTrans	6.782	7.371	7.895	12.454	13.778	_14.648_
DASTNet	6.454	7.461	8.424	12.304	13.960	15.225
MAML	6.765	8.170	8.834	13.227	14.470	16.953
TPB	6.014	7.322	8.571	_9.832_	14.512	16.308
STGFSL	_5.925_	_7.244_	_8.356_	11.157	_13.450_	15.444
GPD	**5.570**	**5.971**	**6.582**	**10.165**	**11.344**	**13.003**

Table 11: Performance comparison of few-shot scenarios on Baltimore dataset at different prediction steps in terms of MAE and RMSE. Bold denotes the best results and underline denotes the second-best results.

	MAE			RMSE		
Model	Step 1	Step 3	Step 6	Step 1	Step 3	Step 6
HA	34.705	34.705	34.705	52.461	52.461	52.461
ARIMA	27.865	27.695	33.771	40.643	45.003	59.359
RegionTrans	16.138	19.318	_22.103_	26.248	32.489	_37.654_
DASTNet	16.480	22.464	27.147	25.788	36.717	43.834
MAML	14.083	19.753	24.493	23.473	33.079	40.407
TPB	16.616	21.835	28.005	**20.50**	_28.386_	37.701
STGFSL	**13.479**	_18.654_	23.054	_21.918_	31.106	37.818
GPD	_13.580_	**16.076**	**18.923**	22.081	**27.329**	**32.260**

Table 12: Performance comparison of few-shot scenarios on NYC dataset at different prediction steps in terms of MAE and RMSE. Bold denotes the best results and underline denotes the second-best results.

	MAE			RMSE		
Model	Step 1	Step 3	Step 6	Step 1	Step 3	Step 6
HA	3.257	3.257	3.257	6.547	6.547	6.547
ARIMA	7.176	7.262	7.114	10.84	11.01	10.89
RegionTrans	2.846	3.278	3.925	4.417	5.729	7.039
DASTNet	2.695	3.205	3.809	4.267	5.516	7.028
MAML	2.756	_3.121_	3.896	4.182	5.584	6.909
TPB	**2.485**	3.129	_3.680_	**4.094**	_5.513_	_6.816_
STGFSL	2.679	3.187	3.686	4.147	5.599	6.987
GPD	_2.587_	**3.098**	**3.674**	_4.135_	**5.502**	**6.715**

Table 13: Performance comparison of few-shot scenarios on METR-LA dataset at different prediction steps in terms of MAE and RMSE. Bold denotes the best results and underline denotes the second-best results.

	MAE			RMSE		
Model	Step 1	Step 3	Step 6	Step 1	Step 3	Step 6
HA	3.142	3.142	3.142	4.535	4.535	4.535
ARIMA	5.179	5.456	5.413	6.829	7.147	7.144
RegionTrans	2.388	2.845	3.071	3.464	4.166	4.488
DASTNet	2.278	2.818	3.164	3.256	3.909	4.427
MAML	2.396	2.885	3.181	3.327	4.050	4.499
TPB	2.156	2.593	3.116	_3.082_	_3.637_	4.382
STGFSL	_2.133_	_2.565_	_2.901_	3.183	3.815	_4.291_
GPD	**2.031**	**2.381**	**2.550**	**2.948**	**3.422**	**3.630**

Table 14: Performance comparison of few-shot scenarios on Didi-Chengdu dataset at different prediction steps in terms of MAE and RMSE. Bold denotes the best results and underline denotes the second-best results.